APL Photonics

Optical parametric gain in CMOS-compatible sub-100 μm photonic crystal waveguides

Cite as: APL Photonics **5**, 066108 (2020); https://doi.org/10.1063/5.0003633
Submitted: 03 February 2020 • Accepted: 03 June 2020 • Published Online: 22 June 2020

Ezgi Sahin, Doris K. T. Ng and Dawn T. H. Tan

Optical parametric gain in CMOS-compatible sub-100 μm photonic crystal waveguides

Cite as: APL Photon. 5, 066108 (2020); doi: 10.1063/5.0003633
Submitted: 3 February 2020 • Accepted: 3 June 2020 •
Published Online: 22 June 2020

Ezgi Sahin,[1,a] Doris K. T. Ng,[2] and Dawn T. H. Tan[1,b]

AFFILIATIONS

[1] Photonics Devices and Systems Group, Engineering Product Development, Singapore University of Technology and Design (SUTD), 8 Somapah Road, Singapore 487372
[2] Institute of Microelectronics, A*STAR, 2 Fusionopolis Way, #08-02, Innovis Tower, Singapore 138634, Singapore

[a] **Current address:** Ecole Polytechnique Fédérale de Lausanne, Photonic Systems Laboratory (PHOSL), STI-IEL, Station 11, CH-1015 Lausanne, Switzerland. **Author to whom correspondence should be addressed:** ezgi_sahin@alumni.sutd.edu.sg
[b] **Electronic mail:** dawn_tan@sutd.edu.sg

ABSTRACT

Emerging compositionally engineered complementary metal-oxide-semiconductor (CMOS)-compatible platforms have been employed for high efficiencies in various on-chip applications, including optical parametric amplification and wavelength conversion. Combining the novel nonlinear optics platforms such as ultra-silicon-rich nitride (USRN: Si_7N_3) with periodic waveguide structures can lead to further enhancement of material nonlinearities via the slow light effect and enable ultra-compact devices. Four-wave mixing in a USRN-based, CMOS-compatible, photonic crystal waveguide (PhCWg) leading to on/off optical parametric signal gain reaching 3 dB, and a large instantaneous idler conversion efficiency of −1 dB is explored experimentally. Enhancement of Kerr nonlinearity in the presence of a sizable and near-constant group index allows the findings on an ultra-compact, 97 μm-long PhCWg, equivalent to a large on/off gain per unit length of 333 dB/cm.

I. INTRODUCTION

Nonlinear optics is based on light–matter interactions at power levels sufficiently large to induce a refractive index change for near-instantaneous modulation of optical signals.[1] Prevailing complementary metal-oxide-semiconductor (CMOS)-compatible photonics platforms, i.e., silicon[2] and silicon nitride,[3] are centrosymmetric; therefore, they rely on Kerr nonlinearities that emerge due to the third-order susceptibility ($\chi^{(3)}$) for demonstrating nonlinear optical phenomena. An essential third-order parametric process is four-wave mixing (FWM); it occurs due to nonlinear interactions among four optical waves where the energy and momentum are conserved. FWM is the underlying process of many applications including parametric amplification,[4] optical sampling,[5] all-optical wavelength conversion,[6] and demultiplexing[7] and therefore has an indispensable role in optical signal processing. Moreover, it is used to create entangled photon pairs for quantum communication networks.[8]

Through exploiting both material and structural properties of integrated photonic devices, it is possible to tune the light–matter interactions to a greater extent, allowing the full potential of on-chip nonlinear processes to be efficiently unlocked.[9] One way to engineer the structural properties of a waveguide is by introducing a two-dimensional periodicity on the plane of light propagation, via photonic crystal waveguides.[10] PhCWgs allowed impressive progress in nonlinear optical signal processing applications on the widely used CMOS-compatible silicon platform and led to successful demonstrations of interesting nonlinear photonic phenomena including integrated autocorrelators,[11] temporal compression,[12] third harmonic generation,[13] and four-wave mixing.[14–16]

Material properties play a key role in the efficiency of nonlinear processes. The limitations of the existing CMOS-compatible platforms such as nonlinear losses in silicon, two-photon absorption (TPA) and free-carrier (FC) effects and lower Kerr nonlinearity in stoichiometric silicon nitride, turned the research efforts toward

the exploration of new CMOS-compatible platforms. We created the compositionally engineered ultra-silicon-rich nitride (USRN), possessing a sufficiently large bandgap of 2.1 eV to eliminate two-photon absorption at 1.55 μm with a material composition of Si_7N_3. This composition unlocks an order of magnitude larger Kerr nonlinearity compared to stoichiometric silicon nitride at telecommunication wavelengths in the absence of nonlinear losses. USRN possesses a large Kerr nonlinearity of 2.8 × 10^{-13} cm^2/W and a linear refractive index of 3.1,[4,17] making it ideal for harnessing nonlinear phenomena on CMOS-compatible integrated devices without the need for high input powers. Supercontinuum generation (SCG), optical parametric amplification (OPA), and four-wave mixing have been demonstrated in USRN waveguides with high efficiencies.[4,17,18]

PhCWgs can enhance nonlinear effects through slow light, which is caused by the inverse group velocity scaling with the large group indices brought about by the waveguide periodicity.[10] The enhanced light–matter interaction in PhCWgs allows the reduction in device footprint compared to channel waveguides, where the length scales are at the order of millimeters or centimeters for realizing nonlinear optical processes. However, the complex PhCWg structures lead to larger linear losses, which are commonly tolerated by using compact device footprints. They can also cause an increase in the severity of nonlinear losses such as two-photon absorption (TPA) and free-carrier (FC) absorption, inherent in silicon. This could consequently hinder the efficient implementation of all-optical signal processing on compact photonic chips as they result in undesirable attenuation in optical fields. Here, USRN platform mitigates these nonlinear losses.[4,17] In addition, a group index of 20 is achieved in the PhCWg structure that is symmetrically cladded with SiO_2, eliminating the structural robustness issues associated with air-membrane structures.

We previously demonstrated the design and fabrication of the PhCWgs on the USRN platform with silica over- and under-cladding for better structural robustness and characterized the nonlinear enhancement in our PhCWgs.[19] In this manuscript, we show FWM in a degenerate pump configuration using a pulsed pump and present the large on/off idler conversion efficiency and signal gain in USRN PhCWgs, reaching 333 dB/cm.

II. RESULTS

A. Characterization of photonic crystal waveguide

For the FWM experiments, we used a 97 μm-long PhCWg fabricated on a USRN wafer with 300 nm thickness and with the parameters radius r = 105 nm, row shift s_1 = 40 nm, and lattice constant a = 430 nm. The PhCWg has a propagation loss of 22 ± 2 dB/cm in the slow light region. Fabrication details can be found in the supplementary material, and further information on the device design, fabrication details, and the scaling of effective Kerr nonlinearity can be found elsewhere.[19] Scanning electron micrograph (SEM) taken before the cladding deposition is given in Fig. 1(a). The transmission spectrum of the PhCWg measured using a broadband amplified spontaneous emission (ASE) source and an optical spectrum analyzer is given in Fig. 1(b).

First, we characterize the group index of the PhCWg to infer the wavelength region of the flat-band slow light for our FWM experiments. To do this, we constructed a fiber-based Mach–Zehnder

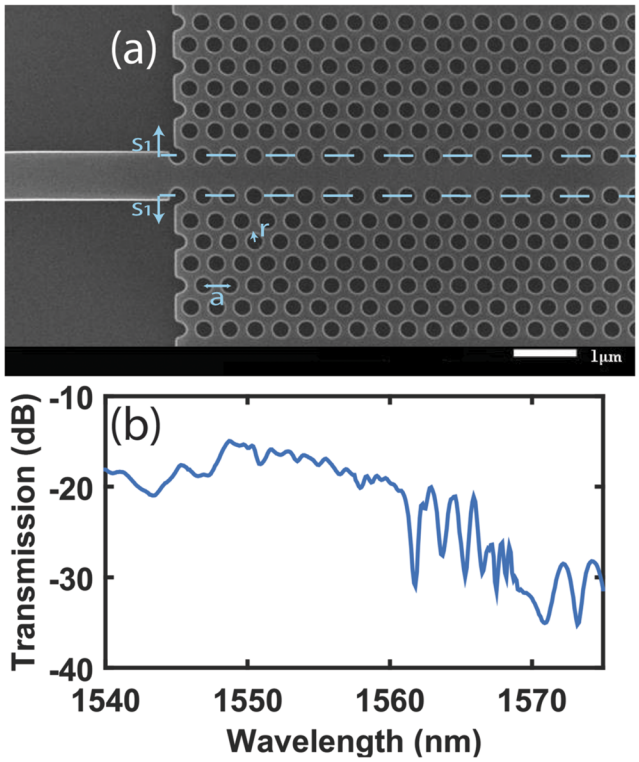

FIG. 1. (a) Scanning electron micrograph of the photonic crystal waveguide (PhCWg) taken before the cladding deposition, showing the PhCWg parameters radius r, row shift s_1, and lattice constant a. (b) Transmission of the PhCWg device normalized with respect to the ASE source.

interferometer (MZI) that is shown in Fig. 2(a). It works by first separating the light from an ASE source into two arms using a coupler. Each arm introduces different group delays to the propagating light before these two arms are combined back with another coupler. The phase difference creates the interference pattern, as shown in Fig. 2(b). This measured spectrum can be used to extract the group delay difference of the test and reference arm as[19]

$$n_{gPhCWg} = \frac{L_{ref} \times n_{gRef} \pm \frac{\lambda^2}{\Delta\lambda_{MZI}}}{L_{PhCWg}}, \quad (1)$$

where L_{ref} and L_{PhCWg} are the length of the reference arm and the photonic crystal waveguide, respectively. $\Delta\lambda_{MZI}$ denotes the fringe spacing in the interference pattern. For an interference pattern with prominent peaks, we used an attenuator, in addition to the 90:10 coupler, to have the same levels of the output power from both MZI arms.

The fibers of different lengths are adjusted at both arms to have the same delay-time; the variable optical delay line (VODL) is used to tune the difference in delay. In our measurement, the reference arm is advanced, i.e., the PhCWg arm is delayed with respect to the reference arm. As the group index of the PhCWg increases toward the band edge, the delay is increased, and the difference of

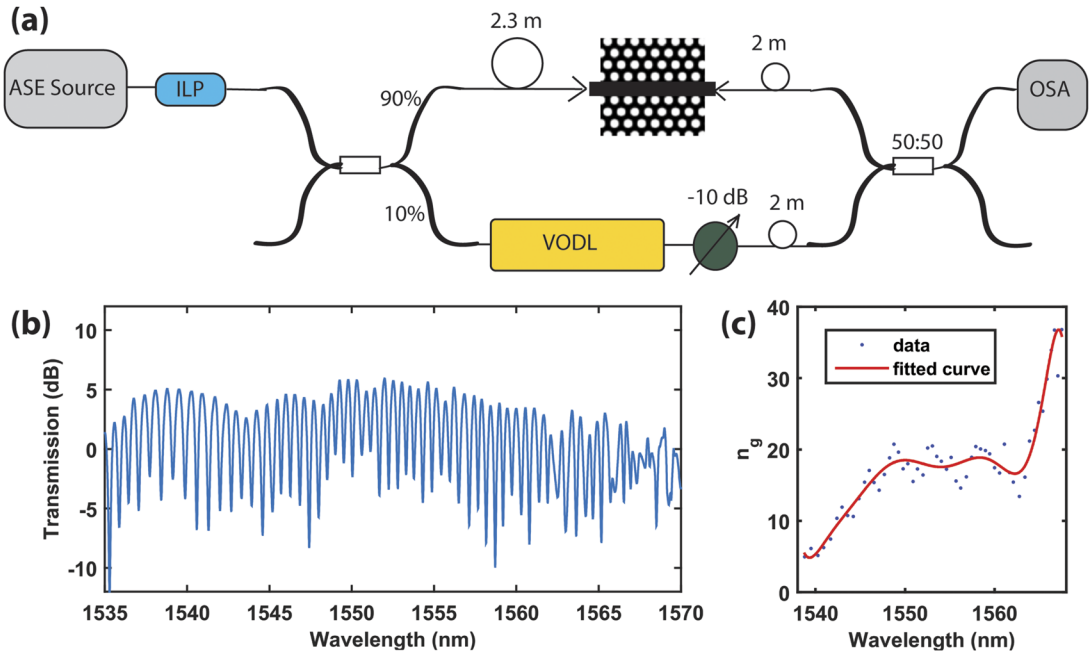

FIG. 2. (a) Schematic of the setup consisting of an amplified spontaneous emission (ASE) source, in-line polarizer (ILP), 90:10 coupler, variable optical delay line (VODL), 10 dB attenuator, fibers, 50:50 coupler, and optical spectrum analyzer (OSA), used to characterize the group index of the PhCWg. (b) Oscillations in the spectrum due to constructive and destructive interference. (c) Group index extracted from the period of oscillations.

delays between the reference arm and the PhCWg arm is reduced. This variation creates the change in oscillation period with respect to frequency; the oscillation period decreases as n_g increases, as seen in Fig. 2(b). To calculate the group index characteristics of the PhCWg, we use Eq. (1) and take the ± sign as a summation during calculation as the reference arm is advanced with respect to the device arm. We obtain the group index curve, as shown in Fig. 2(c), with the 10 nm span flat-band slow light at n_g close to 20. Simulation details, band diagrams, and simulated PhCWg group index curves were previously presented.[19] The red curve is a high order polynomial fit to data to construct a visual guide to eyes. The group index data helps us to determine the operating region for the FWM experiments.

B. Four-wave mixing

To exploit the high group index in a 10 nm span, we operated within the flat-band slow light region. The setup used for FWM experiments is shown in Fig. 3. We performed the measurements in a degenerate pump configuration; for the signal, we used a continuous wave (CW) and tunable laser source, and for the pump, we used a mode-locked laser (MLL) that launches pulses with a full width at half maximum (FWHM) of 9 ps at 20 MHz repetition rate (RP), centered at 1551 nm. An EDFA is used to amplify the signal to increase the visibility of the generated idler by raising it above the noise floor of the optical spectrum analyzer (OSA). To reduce the noise from the sources, both the signal and the pump are filtered using bandpass filters (BPFs), possessing 3 dB bandwidths of 1.5 nm for the

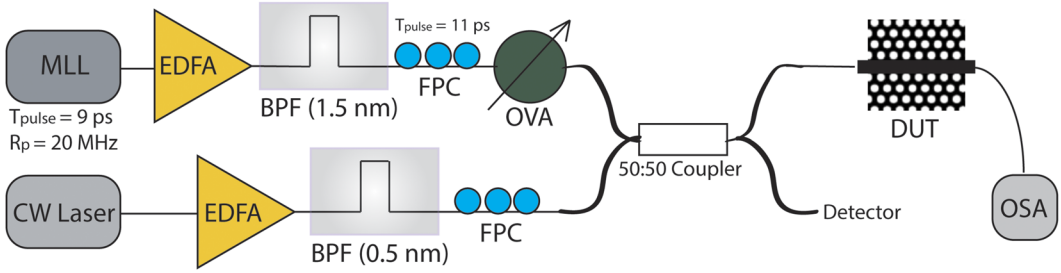

FIG. 3. Schematic of the setup used in the FWM experiments consisting of mode-locked laser (MLL), continuous wave (CW) laser, erbium-doped fiber amplifier (EDFA), bandpass filters (BPFs), fiber polarization controllers (FPCs), optical variable attenuator (OVA), device under test (DUT), and OSA.

pump and 0.5 nm for the signal. After the BPF, the pump FWHM is measured with an autocorrelator to be 11 ps (the time-bandwidth product is 0.57). The variable attenuator is used to change the pump power and observe the variations in the conversion efficiency of the idler as well as the signal gain. To control the polarization and to maintain transverse-electric polarization, we used polarization-maintaining (PM) fibers and components after the fiber polarization controller (FPC) plates. Signal and pump arms are combined using a 50:50 fiber coupler and coupled in and out of the chip via tapered lensed fibers.

Figure 4(a) shows the FWM spectra with varying pump powers. The mixing of two photons from the pump and one from the signal produces one idler photon at the frequency $\omega_i = 2\omega_p - \omega_s$, at a rate equivalent to the pump repetition rate. Another photon is generated at the signal wavelength, which promotes the signal amplification. When using a pulsed pump, the calculation of the instantaneous conversion efficiency (also called on/off idler conversion efficiency) differs from that of the CW pump and signal; the spectrally integrated power from the OSA measurements should be weighted by the duty cycle factor [F = 1/(20 MHz × 11 ps)] to obtain the instantaneous conversion efficiency. The instantaneous response of the Kerr medium leads to idler generation in the presence of the pump, i.e., in a pulsed fashion, leading to an idler possessing high peak powers, therefore high on/off idler conversion efficiencies defined as the ratio between the measured idler power at the output of the photonic crystal waveguide (PhCWg) with the pump on and the signal power at the output of the PhCWg with the pump off.[4,20]

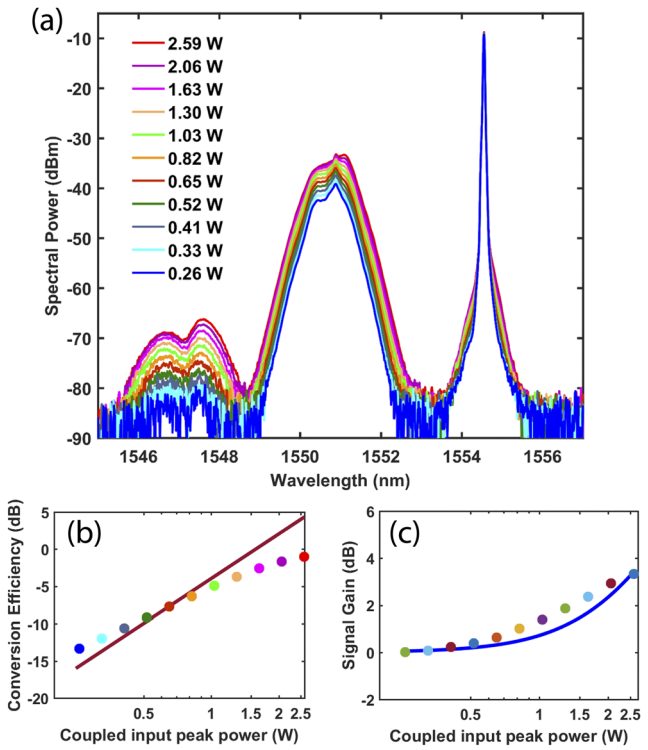

FIG. 4. (a) FWM spectra recorded with the OSA with varying input peak powers when the CW signal is centered at 1554.6 nm; the colors shown in the legend denote the input peak power coupled in the PhCWg. (b) Calculated (dark red line) and measured (colored circles) idler conversion efficiency as a function of coupled input peak power. (c) Calculated (blue line) and measured (colored circles) signal gain as a function of coupled input peak power. Horizontal axes for (b) and (c) are plotted on a logarithmic scale.

We derived the on/off idler conversion efficiency and signal gain, as shown in Figs. 4(b) and 4(c), with the colored filled circles, by analyzing the spectra measured by using the optical spectrum analyzer (OSA) with 0.05 nm resolution. We define the on/off idler conversion efficiency as the ratio between the measured idler power at the output of the photonic crystal waveguide (PhCWg) with the pump on and the signal power at the output of the PhCWg with the pump off, namely, $P_{signal,out}$.[4,20] The idler peak power is calculated by taking the integral of $P_{idler,ave}$ and taking the pump pulse repetition rate and pulse width into account, $P_{idler,peak} = \frac{1}{R_p T_{pulse}} \int P_{idler,ave}(\lambda) d\lambda$, where the R_p is the repetition rate of the mode-locked laser and T_{pulse} is the input pulse width of the sech pulses injected into the PhCWg. $P_{idler,ave}(\lambda)$ is the average output power spectrum as a function of the wavelength measured by using the OSA. The calculation of instantaneous idler conversion efficiency in a pulsed degenerate pump configuration is $P_{idler,\,peak}/P_{signal,out}$. The peak power of the signal at the output is calculated by $P_{signal,peak} = \frac{1}{R_p T_{pulse}} \int P_{signal,ave}(\lambda) d\lambda$. We applied a band rejection filter to eliminate the power in the narrowband CW tone of the signal and obtain $P_{signal,ave}$. The on/off optical parametric gain of the signal is then given by $P_{signal,peak}/P_{signal,out}$.

The four-wave mixing conversion efficiency of the idler and the parametric gain of the signal is calculated and plotted together with the measured results in Figs. 4(b) and 4(c). The gain coefficient $g = \left[(\gamma_{eff} P)^2 - \left(\frac{\beta_2 \Omega^2 + 2\gamma_{eff} P}{2}\right)^2\right]^{\frac{1}{2}}$, where γ_{eff} is the effective nonlinear parameter, P is the coupled peak power of the pump, β_2 is the group velocity dispersion, and Ω is the detuning between the pump and the signal.[15,25] The conversion efficiency of the four-wave mixing process is calculated using the expression, $CE = (\gamma_{eff} P \sinh(gL)/g)^2 . e^{-\alpha L}$, whereas the parametric gain of the signal $G_{signal} = 1 + CE$. The loss parameter is $\alpha = 510\ m^{-1}$ and $\gamma_{eff} = 5.5 \times 10^3\ W^{-1}/m$. In calculating the conversion efficiency, we assume an undepleted pump and the absence of two-photon absorption, which has been experimentally verified in USRN using both z-scan and waveguide experiments.[17,21]

The slow-down factor, $S = n_g/n_0$, accounts for the slow-light scaling of nonlinear effects, where $\gamma_{eff} = \gamma S^2$ scales with S^2, and the reduced group velocity for the light propagating through the waveguide is given by $v_g = c/n_g$. S. Light spends more time confined in the periodic waveguide due to its slower group velocity, leading to enhanced light–matter interaction and, therefore, large on/off idler conversion efficiency and on/off signal gain (Figs. 4 and 5). Utilizing carefully designed periodic waveguide structures, scaling of nonlinear effects with large group indices can allow for shorter device lengths and lower powers to initiate nonlinear processes. Nevertheless, slow-light scaling also acts to exacerbate nonlinear losses such as TPA that are prominent in silicon,[9] which are absent in USRN through meticulous material composition engineering as previously mentioned.[4] The USRN TPA edge has previously been characterized to exist at 1.2 μm, above which TPA is absent,[22] but 3 PA can still exist in the telecommunication wavelengths.[4,17] We, therefore,

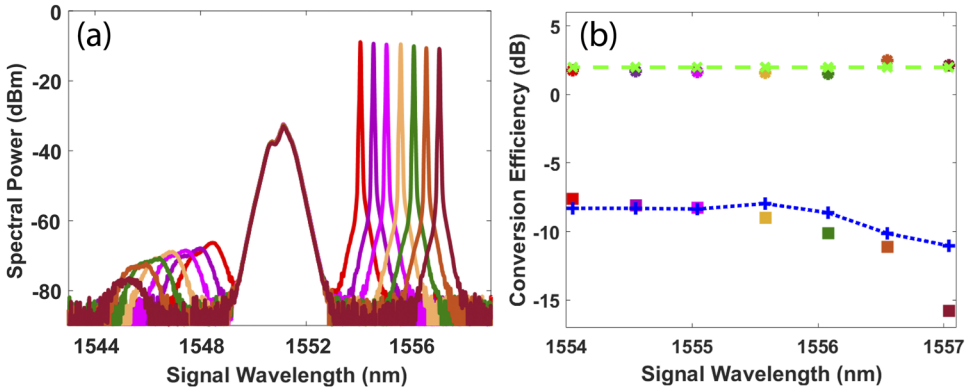

FIG. 5. (a) FWM spectra measured by using the OSA with varying signal wavelengths with a fixed pump peak power of 1.17 W; the colors correspond to the respective points in (b). (b) Instantaneous idler conversion efficiency and signal gain with respect to the varying signal wavelength. The calculated signal gain and idler conversion efficiency are shown as green crosses (×) and blue crosses (+), respectively.

believe that the discrepancy between the slopes of the calculated and measured CE is a result of the non-trivial scaling of three-photon absorption in PhCWgs, as previously reported in GaInP PhCWgs.[21]

Engineering the PhCWg with row shifts allows for a wider operational bandwidth for the FWM. Maintaining the same pump wavelength as the demonstrations in Fig. 4, we altered the signal wavelength with 0.5 nm increments. The measured spectra are given in Fig. 5(a), and the calculated and measured instantaneous idler conversion efficiency and signal gain are given in Fig. 5(b). Since the signal wavelength is still within the flat-band slow light region within our measurement range, the signal gain does not vary substantially. The group index, n_g, of the idler varies considerably as the signal wavelength is changed, contributing to the decrease in the idler conversion efficiency as the signal wavelength is increased; this is one of the factors that contribute to the discrepancy of the calculated and measured CE. Even though the signal does not experience a substantial fluctuation in n_g, the generated idler starts experiencing a lower n_g as the signal wavelength is red shifted. In deriving the idler conversion efficiency from the measured data, the transmission level of the idler, as represented in Fig. 1(b), is also playing a role. Since the idler conversion efficiency by definition refers to the idler power with respect to the signal power at the waveguide output, the decreasing transmission of the PhCWg from 1548 nm to 1543 nm will likewise result in a reduction in the idler conversion efficiency as the signal wavelength increases. The discrepancy in the last data point for the CE in Fig. 5(b) is also explained with this increase in the linear losses. As explained further in the supplementary material, the larger propagation losses shown in Fig. 1(b) at the blue side of the flat-band slow light region can be related to the extent of the light cone[19,23] and further explains the discrepancy in the CE data point at 1557 nm. Overall, the measured and calculated signal gain and conversion efficiency as a function of signal wavelength for a fixed pump wavelength of 1551 nm show good agreement between the calculated and measured values. It is also useful to note that due to the small pump-signal detuning, the impact of phase mismatch on the gain/conversion efficiency is negligible mainly because the device length is also short. Therefore, the phase mismatch accumulated over the 97 μm device length is small.

III. DISCUSSION

Due to the flat-band slow light created by the PhCWg periodicity, we were able to observe a substantial on/off idler conversion efficiency up to −1 dB at the input coupled peak power of 2.5 W. In previous demonstrations with USRN channel waveguides, the linear relationship between the coupled input peak power and the output power has been demonstrated for power levels up to 800 W and input peak optical intensities up to 50 GW/cm^2.[17] Since the limit imposed by the TPA on the efficiency of the optical parametric amplification (OPA) process is absent in USRN; we were able to achieve high conversion. Besides, the absence of a blue shift in the pump indicates lack of free-carrier dispersion.[15]

Previous studies on four-wave mixing and parametric amplifiers on GaInP photonic crystal waveguides[24–26] have demonstrated good device performance reaching an on-chip gain of 11 dB.[24] These inspiring works were supported by air-membrane 1.5 mm long PhCWgs that were not CMOS-compatible. Comparing this to our results, we can infer that fabricating longer USRN PhCWgs might lead to better device performance at the cost of larger footprints. Nevertheless, there exists an inherent trade-off for PhCWg structures: they allow the small footprints at the cost of larger propagation losses compared to channel waveguides. The high gain per unit length factor is, therefore, partially attributed to the small footprint of the device. The signal gain per unit length in the USRN PhCWgs demonstrated here is 333 dB/cm, whereas the aforementioned results in GaInP have a signal gain of 73 dB/cm.[24] With reference to the parametric gain in photonic waveguides at a wavelength of 1550 nm, 42.5 dB gain has been demonstrated in USRN waveguides with a length of 7 mm, implying a length normalized gain of 60.7 dB/cm.[4] Comparing the normalized gain demonstrated here in the USRN PhCWg, gain per unit length is significantly larger than that in the USRN waveguide. The origin of this large gain enhancement is the elevated group index, induced close to the band edge, by the photonic crystal structure.

Hybrid slot waveguide schemes that use a separate gain medium have also been demonstrated recently; a modal gain of 52.4 dB/cm was reported in a CMOS-compatible device using Si_3N_4 slot waveguides with Erbium as the gain medium deposited within the slot.[27] In our work, higher gain per length comes at the cost of reduced bandwidth compared to channel or slot waveguides; however, it drastically reduces the device footprint. Hybrid structures can also be fabricated with photonic crystal structures, as theoretically proposed on silicon slotted PhCWg with silicon

nanocrystal material embedded in silica host (SiNC/SiO_2) for its large Kerr nonlinearity.[28]

It is meaningful to note an essential figure-of-merit for PhCWgs used for optical signal processing; group index—bandwidth product, $n_g(\Delta\omega/\omega)$. Bandwidth limits the detuning for FWM experiments, while n_g is a measure for slow-light enhancement of nonlinear effects, which enhances the conversion efficiency and signal gain in FWM. We calculated $n_g(\Delta\omega/\omega)$ for our PhCWg to be 0.2. Previous demonstration of row-shifted PhCWgs in silicon reached ~0.3, which came with the cost of fabricating air-suspended PhCWgs, compromising on the device robustness and CMOS-compatibility.[29] Yet, the PhCWg design demonstrated here with the silica cladding can be used in larger CMOS-compatible systems.

In our device, the field is coupled into the 97 μm-long PhCWg via an access waveguide, which is short in the design to minimize their contribution to the CE. The length of the input access waveguide at the input is 200 μm. The slow light enhancement factor, S^2, is $(4/3.1)^2 = 1.7\times$ for the access waveguide and $S^2 = 37.6$ for the PhCWg, as calculated from the measured group index data in Fig. 2(c). Based on the contribution to the acquired nonlinear phase ($\Delta\varphi_{NL} = \gamma_{eff}\boldsymbol{P_{in}L}$) from the waveguide length and nonlinear parameter, the contribution from the access waveguide is 11× less than that from the PhCWg.

As the field of integrated photonics moves toward utilizing optical nonlinearities toward single photons for quantum applications, it is becoming necessary to induce nonlinear effects at low power levels. Consequently, our results are promising for the generation of correlated photon pairs with USRN PhCWgs.

IV. CONCLUSION

The high nonlinear figure-of-merit (FOM) of USRN[17] originates from its high Kerr nonlinearity of $n_2 = 2.8 \times 10^{-13}$ cm^2/W and lack of TPA and FC effects. The nonlinearity of this platform is further enhanced by engineering the PhCWg structure for the sizable group index over a wide flat band. To capitalize on the experimentally observed large nonlinearity in USRN-based PhCWgs,[19] we performed FWM experiments in a degenerate pump configuration with a continuous wave signal and pulsed pump with 20 MHz repetition rate. We observed parametric wavelength conversion at low operating powers of a few Watts and an ultra-short device length of 97 μm. In the low power regime and ultra-compact device, an instantaneous idler conversion efficiency reaching −1 dB is observed, as well as parametric amplification of signal reaching 3 dB, corresponding to a gain per length figure of 333 dB/cm. Furthermore, this realization is on a back-end CMOS-compatible platform with SiO_2 cladding, which improves the device robustness compared to air-membrane structures. More on-chip functionalities that are lacking in the integrated photonics toolkit can be discovered by combining structurally engineered waveguides with novel nonlinear materials such as USRN.

SUPPLEMENTARY MATERIAL

See the supplementary material for further details.

ACKNOWLEDGMENTS

This work was supported by the National Research Foundation Competitive Research Grant, MOE ACRF Tier 2 grant, AI Partnership Grant, SUTD–MIT International Design Center, and the Digital Manufacturing and Design grant. The authors acknowledge the National Research Foundation, Prime Minister's Office, Singapore, under its Medium-Sized Centre Program.

DATA AVAILABILITY

The data that support the findings of this study are available from the corresponding author upon reasonable request.

REFERENCES

[1] J. Leuthold, C. Koos, and W. Freude, Nat. Photonics **4**, 535 (2010).
[2] K. Narayanan and S. F. Preble, Opt. Express **18**, 8998 (2010).
[3] C. J. Krückel, A. Fülöp, T. Klintberg, J. Bengtsson, P. A. Andrekson, and V. Torres-Company, Opt. Express **23**, 25827 (2015).
[4] K. J. A. Ooi, D. K. T. Ng, T. Wang, A. K. L. Chee, S. K. Ng, Q. Wang, L. K. Ang, A. M. Agarwal, L. C. Kimerling, and D. T. H. Tan, Nat. Commun. **8**, 13878 (2017).
[5] L. K. Oxenlowe, H. Ji, M. Galili, M. Pu, H. Hu, H. C. H. Mulvad, K. Yvind, J. M. Hvam, A. T. Clausen, and P. Jeppesen, IEEE J. Sel. Top. Quantum Electron. **18**, 996 (2012).
[6] M. A. Foster, A. C. Turner, R. Salem, M. Lipson, and A. L. Gaeta, Opt. Express **15**, 12949 (2007).
[7] F. Li, M. Pelusi, D.-X. Xu, A. Densmore, R. Ma, S. Janz, and D. J. Moss, Opt. Express **18**, 3905 (2010).
[8] S. Clemmen, K. P. Huy, W. Bogaerts, R. G. Baets, P. Emplit, and S. Massar, Opt. Express **17**, 16558 (2009).
[9] C. Monat, B. Corcoran, M. Ebnali-Heidari, C. Grillet, B. J. Eggleton, T. P. White, L. O'Faolain, and T. F. Krauss, Opt. Express **17**, 2944 (2009).
[10] T. Baba, Nat. Photonics **2**, 465 (2008).
[11] C. Monat, C. Grillet, M. Collins, A. Clark, J. Schroeder, C. Xiong, J. Li, L. O'Faolain, T. F. Krauss, B. J. Eggleton, and D. J. Moss, Nat. Commun. **5**, 3246 (2014).
[12] A. Blanco-Redondo, C. Husko, D. Eades, Y. Zhang, J. Li, T. F. Krauss, and B. J. Eggleton, Nat. Commun. **5**, 3160 (2014).
[13] B. Corcoran, C. Monat, C. Grillet, D. J. Moss, B. J. Eggleton, T. P. White, L. O'Faolain, and T. F. Krauss, Nat. Photonics **3**, 206 (2009).
[14] J. F. McMillan, M. Yu, D.-L. Kwong, and C. W. Wong, Opt. Express **18**, 15484 (2010).
[15] C. Monat, M. Ebnali-Heidari, C. Grillet, B. Corcoran, B. J. Eggleton, T. P. White, L. O'Faolain, J. Li, and T. F. Krauss, Opt. Express **18**, 22915 (2010).
[16] J. Li, L. O'Faolain, I. H. Rey, and T. F. Krauss, Opt. Express **19**, 4458 (2011).
[17] T. Wang, D. K. T. Ng, S.-K. Ng, Y.-T. Toh, A. K. L. Chee, G. F. R. Chen, Q. Wang, and D. T. H. Tan, Laser Photonics Rev. **9**, 498 (2015).
[18] J. W. Choi, B. U. Sohn, G. F. R. Chen, D. K. T. Ng, and D. T. H. Tan, Appl. Phys. Lett. **112**, 181101 (2018).
[19] E. Sahin, K. J. A. Ooi, G. F. R. Chen, D. K. T. Ng, C. E. Png, and D. T. H. Tan, Appl. Phys. Lett. **111**, 121104 (2017).
[20] X. Liu, R. M. Osgood, Y. A. Vlasov, and W. M. J. Green, Nat. Photonics **4**, 557 (2010).
[21] C. Husko, S. Combrié, Q. V. Tran, F. Raineri, C. W. Wong, and A. De Rossi, Opt. Express **17**, 22442 (2009).
[22] B.-U. Sohn, J. W. Choi, D. K. T. Ng, and D. T. H. Tan, Sci. Rep. **9**, 10364 (2019).
[23] C. Jamois, R. B. Wehrspohn, L. C. Andreani, C. Hermann, O. Hess, and U. Gösele, Photonics Nanostruct. - Fundam. Appl. **1**, 1 (2003).

[24]I. Cestier, S. Combrié, S. Xavier, G. Lehoucq, A. De Rossi, and G. Eisenstein, Opt. Lett. **37**, 3996 (2012).
[25]I. Cestier, A. Willinger, P. Colman, S. Combrié, G. Lehoucq, A. De Rossi, and G. Eisenstein, Opt. Lett. **36**, 3936 (2011).
[26]P. Colman, I. Cestier, A. Willinger, S. Combrié, G. Lehoucq, G. Eisenstein, and A. De Rossi, Opt. Lett. **36**, 2629 (2011).
[27]J. Rönn, W. Zhang, A. Autere, X. Leroux, L. Pakarinen, C. Alonso-Ramos, A. Säynätjoki, H. Lipsanen, L. Vivien, E. Cassan, and Z. Sun, Nat. Commun. **10**, 432 (2019).
[28]S. Kumar and M. Sen, J. Opt. Soc. Am. B **35**, 362 (2018).
[29]J. Li, T. P. White, L. O'Faolain, A. Gomez-Iglesias, and T. F. Krauss, Opt. Express **16**, 6227 (2008).